Regulation of lactate production at the onset of ischaemia is independent of mitochondrial NADH/NAD$^+$: insights from *in silico* studies

Lufang Zhou[1,4], William C. Stanley[2,4], Gerald M. Saidel[1,4], Xin Yu[1,4], Marco E. Cabrera[1,2,3,4]

Departments of [1]Biomedical Engineering, [2]Physiology & Biophysics and [3]Pediatrics, and [4]Center for Modelling Integrated Metabolic Systems, Case Western Reserve University Cleveland, OH 44106, USA

Ischaemia decreases mitochondrial NADH oxidation, activates glycolysis, increases the NADH/NAD$^+$ ratio, and causes lactate production. The mechanisms that regulate anaerobic glycolysis and the NADH/NAD$^+$ ratio during ischaemia are unclear. Although continuous measurements of metabolic fluxes and NADH/NAD$^+$ in cytosol and mitochondria are not possible *in vivo* with current experimental techniques, computational models can be used to predict these variables by simulations with *in silico* experiments. Such predictions were obtained using a mathematical model of cellular metabolism in perfused myocardium. This model, which distinguishes cytosolic and mitochondrial domains, incorporates key metabolic species and processes associated with energy transfer. Simulation of metabolic responses to mild, moderate and severe ischaemia in large animals showed that mitochondrial NADH/NAD$^+$ was rapidly reset to higher values in proportion to the reduced O_2 delivery and myocardial oxygen consumption ($M\dot{V}_{O_2}$). Cytosolic NADH/NAD$^+$, however, showed a biphasic response, with a sharp initial increase that was due to activation of glycogen breakdown and glycolysis, and corresponded with lactate production. Whereas the rate of glycolysis and the malate–aspartate shuttle had a significant effect on the cytosolic NADH/NAD$^+$, their effects on the mitochondrial NADH/NAD$^+$ were minimal. In summary, model simulations of the metabolic response to ischaemia showed that mitochondrial NADH/NAD$^+$ is primarily determined by O_2 consumption, while cytosolic NADH/NAD$^+$ is largely a function of glycolytic flux during the initial phase, and is determined by mitochondrial NADH/NAD$^+$ and the malate–aspartate shuttle during the steady state.

(Received 20 June 2005; accepted after revision 10 October 2005; first published online 13 October 2005)
Corresponding author M. E Cabrera: Pediatric Cardiology, Rainbow Babies and Children's Hospital 11100 Euclid Avenue, RBC-389 Cleveland, OH 44106-6011, USA. Email: mec6@case.edu

In cardiomyocytes NADH is primarily formed in the mitochondria by pyruvate and fatty acid oxidation and by the tricarboxylic acid (TCA) cycle, and is oxidized by complex I to fuel the electron transport chain and drive ATP synthesis by oxidative phosphorylation. NADH is also formed in the cytosol by glycolysis and lactate oxidation, and subsequently oxidized while being transported into the mitochondria by the malate–aspartate shuttle, or when coupled with the conversion of pyruvate to lactate. Under normal perfusion conditions, NADH generated by glycolysis and lactate oxidation is transported into the mitochondria through the malate–aspartate shuttle and oxidized by the electron transport chain. With reduced blood flow and oxygen delivery, however, oxygen consumption is lower leading to a higher mitochondrial NADH/NAD$^+$. Ischaemia also activates glycogen breakdown, accelerates glycolysis, and increases lactate production (Stanley *et al.* 1992), resulting in increased oxidation of NADH in the cytosol. Accumulation of lactate and the associated acidosis during ischaemia contributes to cardiac dysfunction and clinical symptoms (Williamson *et al.* 1976). Thus, understanding the mechanisms that control cytosolic NADH/NAD$^+$ and lactate metabolism is of fundamental importance.

During ischaemia, mitochondrial NADH/NAD$^+$ appears to be set by the rate of oxygen consumption and substrate dehydrogenase flux. The mechanism controlling cytosolic NADH/NAD$^+$, however, is less clear (Zhou *et al.* 2005). At present, no reliable methods exist for distinct *in vivo* measurements of NADH/NAD$^+$ and metabolic fluxes in cytosol and mitochondria. As an alternative, computational models can be used to simulate the dynamic metabolic responses in the cytosol and mitochondria in response to blood-flow reduction. For this purpose,

 DOI: 10.1113/jphysiol.2005.093146

a multidomain computational model of cardiac energy metabolism in large animals has been developed that distinguishes transport and metabolic processes in blood, cytosol and mitochondria (Zhou *et al.* 2005). This model simulated the dynamics of key metabolites from swine myocardium under normal and ischaemic conditions observed experimentally. Furthermore, model simulations predicted dynamic responses of chemical species and fluxes in cytosol and mitochondria during ischaemia that could not be measured with current techniques. Up to this point, the model did not distinguish the key steps in the electron transport chain and oxidative phosphorylation, specifically NADH/$FADH_2$ oxidation and ADP phosphorylation. Computational models of cardiac mitochondrial metabolism and electrophysiology have been developed (Korzeniewski, 2000; Cortassa *et al.* 2003) that include these key steps, but do not include cytosolic metabolism and fatty acid oxidation. A model that incorporates both mitochondrial and cytosolic processes is essential for understanding the role of subcellular compartmentation in the regulation of the NADH/NAD^+ ratio and glycolysis during ischaemia.

The overall goal of the present study was to investigate the changes in cytosolic and mitochondrial NADH/NAD^+ ratios and their roles in the differential regulation of cardiac energy metabolism in these two compartments during ischaemia. We modified our previous model by including the proton pumps of the electron transport chain and oxidative phosphorylation, and used it to simulate the metabolic responses to a series of step-wise reductions in blood flow. The simulation results allowed assessment of the differences between cytosolic and mitochondrial NADH/NAD^+ ratios, and the role of glycolysis in setting the cytosolic NADH/NAD^+ ratio and regulating lactate metabolism during ischaemia. We hypothesized that the activation of glycogenolysis and glycolysis during ischaemia affect cytosolic NADH and lactate production, but do not alter mitochondrial NADH/NAD^+. Furthermore, we proposed that inhibition of the transfer of NADH from the cytosol into the mitochondria *via* the malate–aspartate shuttle impairs metabolic communication between the two compartments and significantly effects cytosolic NADH/NAD^+, but has little effect on mitochondrial NADH/NAD^+. These hypotheses were tested in two *in silico* experiments by examining the metabolic responses to ischaemia when either the initial glycogen concentration or malate–aspartate shuttle activity was changed.

Methods

Model development

To quantitatively investigate the effects of blood flow reduction on cardiac energetics and the differential regulation of energy production and utilization in the cytosol and mitochondria, we modified the model of Zhou *et al.* (2005) by including major components in oxidative phosphorylation (Fig. 1). In general, changes in metabolite concentrations in blood (b), cytosol (c) and mitochondria (m) are described by a mathematical model based on mass balances, passive and carrier-mediated transport processes, and distinctive chemical reactions, especially those involved in energy transfer. In the blood domain, the dynamic mass balance equation for species j can be written as:

$$V_{\mathrm{b}}\frac{\mathrm{d}C_{\mathrm{bj}}}{\mathrm{d}t} = \frac{\dot{Q}(C_{\mathrm{aj}} - C_{\mathrm{bj}})}{F} - J_{\mathrm{b-c,j}} \qquad (1)$$

where V_{b} is the domain volume, $\dot{Q}$ is blood flow, C_{aj} is the arterial concentration of species j, C_{bj} is the blood concentration, F is the mixing factor, and $J_{\mathrm{b-c,j}}$ is the mass transport rate from blood to cytosol.

In the cytosolic domain, the concentration of species j may change as a result of metabolic reactions and mass transfer across the cellular membrane and mitochondrial membrane:

$$V_{\mathrm{cj}}\frac{\mathrm{d}C_{\mathrm{cj}}}{\mathrm{d}t} = R_{\mathrm{cj}} + J_{\mathrm{b-c,j}} - J_{\mathrm{c-m,j}} \qquad (2)$$

where V_{cj} is the effective volume of species j in the cytosol, and C_{cj} is the concentration. R_{cj} is the metabolic reaction rate of species j, and $J_{\mathrm{c-m,j}}$ is the mass transport rate from cytosol to mitochondria.

In the mitochondrial domain, the dynamic mass balance equation for species j is:

$$V_{\mathrm{mj}}\frac{\mathrm{d}C_{\mathrm{mj}}}{\mathrm{d}t} = R_{\mathrm{mj}} + J_{\mathrm{c-m,j}} \qquad (3)$$

where V_{mj} is the effective volume of species j in the mitochondrial domain, C_{mj} is the concentration and R_{mj} is the net reaction rate.

In this modified model, the oxygen consumption fluxes are composed of contributions from NADH (N) and $FADH_2$ (F) oxidation:

$$\phi_{\mathrm{O_2\to H_2O}} = \phi_{\mathrm{O_2\to H_2O,N}} + \phi_{\mathrm{O_2\to H_2O,F}} \qquad (4)$$

Where

$$\phi_{\mathrm{O_2\to H_2O,k}} = V_{\mathrm{O_2\to H_2O,k}}\left[\frac{C_{\mathrm{m,O_2}}}{K_{\mathrm{O_2\to H_2O,k}} + C_{\mathrm{m,O_2}}}\right]$$

$$\left[\frac{RS^+_{\mathrm{m,k}}}{v^+_{\mathrm{m,k}} + RS^+_{\mathrm{m,k}}}\right] \qquad (\mathrm{k} = \mathrm{N, F}),$$

$K_{x-y,v-w}$ and $V_{x-y,v-w}$ are Michaelis-Menten coefficients, RS^+ represents NADH/NAD^+ or $FADH_2$/FAD, and v^+ is the corresponding kinetic coefficient. ATP synthesis by oxidative phosphorylation is controlled by both the proton gradient

across the inner mitochondrial membrane and ADP availability, which can be expressed as:

$$\phi_{\mathrm{ADP}\rightarrow\mathrm{ATP}} = V_{\mathrm{ADP}\rightarrow\mathrm{ATP}}\left[\frac{PG}{(PG)_0 + PG}\right]\left[\frac{PS_{\mathrm{m}}^{-}}{\mu_{\mathrm{m}}^{-} + PS_{\mathrm{m}}^{-}}\right] \quad (5)$$

where the proton gradient across the mitochondrial inner membrane $PG = C_{\mathrm{i,H}}/C_{\mathrm{m,H}}$ is represented by the ratio of the proton concentrations in the intermembrane space (i) and mitochondrial matrix (m). The normal resting value for the proton gradient is $(PG)_0$. The phosphorylation state is represented by $PS_{\mathrm{m}}^{-} = \mathrm{ADP_m}/\mathrm{ATP_m}$, and μ^{-} is the corresponding rate coefficient.

The dynamic mass balance for protons in the mitochondrial intermembrane space is:

$$V_{\mathrm{i}}\frac{\mathrm{d}C_{\mathrm{i,H}}}{\mathrm{d}t} = J^{\mathrm{f}}_{\mathrm{m}\rightarrow\mathrm{i,H}} - J^{\mathrm{f}}_{\mathrm{i}\rightarrow\mathrm{m,H}} - J_{\mathrm{Hleak}} \quad (6)$$

where V_{i} is the effective volume of intermembrane space, $J^{\mathrm{f}}_{\mathrm{m}\rightarrow\mathrm{i,H}}$ is the proton efflux from mitochondrial matrix to intermembrane space, $J^{\mathrm{f}}_{\mathrm{i}\rightarrow\mathrm{m,H}}$ is the proton influx, and J_{leak} is the proton leak through the inner membrane. Under steady-state conditions, the proton efflux accompanying

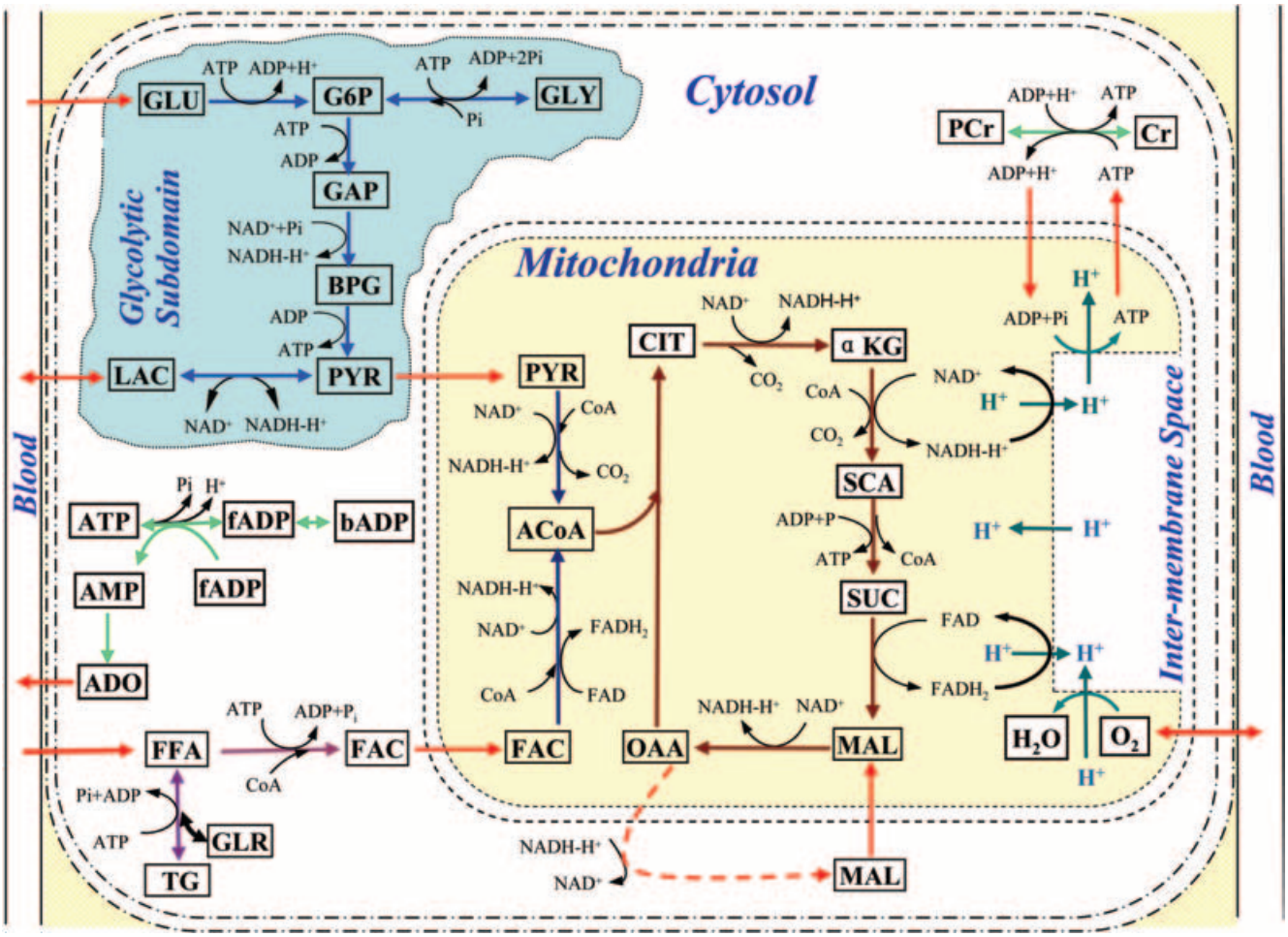

Figure 1. Myocardium metabolic pathway map
This complex network incorporates most key biochemical reactions and pathways involved in cardiac metabolism including glycolysis, pyruvate oxidation, fatty acids oxidation, the tricarboxylic acid (TCA) cycle and oxidative phosphorylation. It also includes species transport across cellular membrane and mitochondrial membrane, as well as proton influx and efflux between mitochondrial matrix and intermembrane space. GLU, glucose; G6P, glucose-6-phosphate; GLY, glycogen; GAP, glyceraldyhe-3-phosphate; BPG, 1,3-bisphosphate-glycerate; PYR, pyruvate; LAC, lactate; TG, triglyceride; GLR, glycerol; FFA, free fatty acid; FAC, fatty acyl-CoA; PCr, phosphocreatine; Cr, creatine; CIT, citrate; α-KG, α-ketoglutarate; SCA, succinyl-CoA; SUC, succinate; MAL, malate; OAA, oxaloacetate; ACoA, acetyl-CoA; bADP, bound ADP; fADP, free ADP; ADO, adenosine.

Table 1. Reaction and transport fluxes values (μmol min^{-1} (g ww)$^{-1}$) involved in oxidative phosphorylation under normal, steady-state conditions

Flux	$\phi_{O_2\rightarrow H_2O,N}$	$\phi_{O_2\rightarrow H_2O,F}$	$\phi_{ADP\rightarrow ATP}$	$J^{f}_{i\rightarrow m,H}$	$J^{f}_{m\rightarrow i,H}$	J_{Hleak}
Value	4.00	1.41	29.63	88.89	96.88	7.99

the oxidation of the reducing equivalents can be obtained by assuming 10 and 6 protons pumped by each NADH and $FADH_2$ oxidation, respectively (Horton *et al.* 2002):

$$J^{f}_{m\rightarrow i,H} = 20\phi_{O_2\rightarrow H_2O,N} + 12\phi_{O_2\rightarrow H_2O,F} \quad (7)$$

Three protons have to pass through the ATP synthase in order to synthesize one ATP (Horton *et al.* 2002); therefore, the accompanying proton influx is

$$J^{f}_{i\rightarrow m,H} = 3\phi_{ADP\rightarrow ATP} \quad (8)$$

The proton leakage through the inner membrane is considered to be a function of the proton gradient across the inner mitochondrial membrane:

$$J^{leak}_{i\rightarrow m,H} = T^{leakage}_{i\rightarrow m,H}\frac{PG}{M^{leakage}_{i\rightarrow m,H} + PG} \quad (9)$$

where $T^{leakage}_{i\rightarrow m,H}$ is a leakage rate coefficient, and $M^{leakage}_{i\rightarrow m,H}$ is the affinity coefficient. Since the affinity coefficient $M^{leakage}_{i\rightarrow m,H}$ is much larger than $(PG)_0$, eqn (9) can be simplified as a quasi-exponential function of ΔpH (Korzeniewski *et al.* 2005), i.e.

$$J^{leak}_{i\rightarrow m,H} = \frac{T^{leakage}_{i\rightarrow m,H}\times PG}{M^{leakage}_{i\rightarrow m,H}} = k_1 e^{k_2\Delta pH}.$$

In cardiac tissue, the transport of NADH from cytosol to mitochondria in exchange for NAD is through the malate–aspartate shuttle, since the mitochondrial inner membrane is not permeable to this coenzyme (Arnold, 1992). This shuttle involves not only oxidation and reduction reactions, but also enzymatic transporters. In the current model, this shuttle is simply expressed as the function of cytosolic and mitochondrial NADH/NAD^+ ratios due to the deficiency of experimental data:

$$J^{f}_{c\rightarrow m,NADH} = T_{c\rightarrow m,NADH}\left[\frac{RS^{+}_{c}}{M_{c,NADH/NAD^+} + RS^{+}_{c}}\right]\left[\frac{RS^{-}_{m,N}}{M_{m,NAD^+/NADH} + RS^{-}_{m,N}}\right] \quad (10)$$

where $T_{c\rightarrow m,NADH}$ is the transport rate coefficient, $M_{m,NAD/NADH}$ and $M_{c,NADH/NAD}$ are the affinity coefficients, RS^{+}_{c} represents the cytosolic NADH/NAD^+ ratio, and $RS^{-}_{m,N}$ represents the mitochondrial NAD^+/NADH ratio.

The healthy heart maintains high ATP and low ADP concentrations with the help of the creatine kinase and adenylate kinase reactions. However, during ischaemia, ADP degrades to AMP and adenosine, and is transported to the extracellular space, resulting in a fall in the total purine nucleotide pools (Ingwall, 2002). In the present model, we incorporated the reactions of adenylate kinase, AMP breakdown and loss of adenosine (Fig. 1). The loss of adenosine was assumed to occur only during ischaemia, and its rate was described as a function of the adenosine concentration change ($\Delta C_{ADO} = C_{ADO} - C_{ADO,0}$): $\phi_{ADOlost} = \frac{100(C_{ADO}-C_{ADO,0})}{C_{ADO}-C_{ADO,0}+5000}$. The corresponding reaction parameters are listed in Table 3.

Parameter estimation and model simulations

The flux values involved in oxidative phosphorylation are determined by flux balance analysis under resting steady-state conditions (Table 1). The initial values of species concentration (in blood, cytosol and mitochondria), transport flux and reaction flux were those used previously (Zhou *et al.* 2005) unless listed in the tables. With the additional oxidative phosphorylation pathways, we modified the reaction flux parameter (Table 2) and some transport flux parameters (Table 3). Parameters and variables that are new or modified are listed in Table 4.

Simulations were orientated to investigate the changes of NADH/NAD^+ and the differential regulation of metabolic processes inside cytosol and mitochondria during the transition from normal to ischaemic conditions. These simulations emphasized the time profiles of key metabolite concentrations (e.g. NADH, NAD^+, glycogen, lactate, etc.) and fluxes (e.g. oxygen consumption, glycolysis, malate–aspartate shuttle, etc.) of mild, moderate and severe ischaemia, and were compared with previously published experimental data in pigs (Salem *et al.* 2004). Corresponding to mild, moderate or severe ischaemia, myocardial blood flow ($\dot{Q}$) was reduced from its normal value of 1.0 ml g^{-1} min^{-1} to 0.7, 0.4 and 0.1 ml g^{-1} min^{-1}, respectively, over 60 s in a linear manner. In addition, *in silico* experiments were performed to test our hypotheses concerning the effects of initial glycogen concentration and malate–aspartate shuttle activity on cytosolic and mitochondrial NADH/NAD^+. Computer simulations were obtained by solving the model equations using DLSODE, a robust implicit integrator for stiff and sparse systems (CASC, 2003; http://www.llnl.gov/CASC/odepack/software/dlsode.f).

Table 2. Reactions fluxes parameter values under normal, steady state

Reactions	$V_{x-y,v-w}$	$K_{x-y,v-w}$	$\mu^{\pm}$	$\nu^{\pm}$
$\phi_{GLU,G6p}$	3.84	8.4	0.088 (+)	0
$\phi_{G6P,GLY}$[1]	0.22	0.017	60 (+)	0
$\phi_{GLY-Pi,G6P}$[2]	2.66	47†, 1.63§	4.2×10^{-4} (–)	0
$\phi_{G6P,GAP}$	4.80	3.25	0.018 (+)	0
$\phi_{GAP,BGP}$	7.76	0.40	0	0.2 (–)
$\phi_{BPG,PRY}$	7.76	0.6	1.1×10^{-4} (–)	0
$\phi_{PYR,LAC}$	4.99	0.002	0	0.9 (+)
$\phi_{LAC,PYR}$	2.17	8.13	0	14 (–)
$\phi_{PYR-CoA,ACoA}$	2.82	0.0014	0	10.76 (–)
$\phi_{TG,GLR}$	0.04	4.27	0	0
$\phi_{GLR-FFA,TG}$	0.12	3.3×10^{-4}	0.088 (+)	0
$\phi_{FA-CoA,FAC}$	1.56	0.015	0.88 (+)	0
$\phi_{FAC-CoA,ACoA}$	2.77	0.033	0	0.86 (–), 4.42 (–)*
$\phi_{ACoA,CIT}$	14.8	1.9×10^{-4}	0	0
$\phi_{CIT,\alpha KG}$	22.2	10.14	0	8.61 (–)
$\phi_{\alpha KG-CoA.SCA}$	22.2	0.51	0	8.61 (–)
$\phi_{SCA,SUC}$	8.14	0.099	0.12 (–)	0
$\phi_{SUC,MAL}$	3.05	0.058	0	4.42 (–)
$\phi_{MAL,OAA}$	22.2	2.82	0	8.61 (+)
$\phi_{PCR,CR}$	8	1.18	0.0011 (–)	0
$\phi_{CR,PCR}$	8	0.5	8.82 (+)	0
$\phi_{ADP,bADP}$	140	0.02	0	0
$\phi_{bADP,ADP}$	5000	73.99	0	0
$\phi_{AMP,ADP}$[3]	150.02	3.8×10^{-4}	0.0088	—
$\phi_{ADP,AMP}$[4]	10001	5.049	1.0×10^{-6}	—
$\phi_{AMP,ADO}$[5]	2000	0.074	—	—
$\phi_{ADO,AMP}$[6]	30	2.5×10^{-4} ‡	—	—
$\phi_{O_2,H_2O.N}$	39.95	0.9627	—	0.93 (+)
$\phi_{O_2,H_2O.F}$	22.64	0.9627	—	0.79 (+)*
$\phi_{fADP,ATP}$	1493.32	—	0.012	$(PG)_0 = 122.50$
$\phi_{ATP,fADP}$	157.10	18	—	—

[1]Glycogen synthesis: $\phi_{G6P-GLY} = \dfrac{V_{G6P,GLY}C_{G6P}}{(K_{G6P}+C_{G6P})}\dfrac{C_{ATP,c}/C_{AMP,c}}{\mu^{+}_{c,AMP}+C_{ATP,c}/C_{AMP,c}}$

[2]Glycogen breakdown: $\phi_{GLY-P_i,G6P} = \dfrac{V_{GLY-P_i,G6P}C_{GLY}C_{P_i}}{(K_{GLY,G6P}+C_{GLY})(K_{P_i,G6P}+C_{P_i})}\dfrac{C_{AMP,c}/C_{ATP,c}}{\mu^{-}_{c,AMP}+C_{AMP,c}/C_{ATP,c}}$

[3]AMP to ADP: $\phi_{AMP-ADP} = \dfrac{V_{AMP,ADP}C_{AMP}}{(K_{AMP,ADP}+C_{AMP})}\dfrac{C_{ATP,c}/C_{ADP,c}}{\mu^{+}_{c}+C_{ATP,c}/C_{ADP,c}}$

[4]ADP to AMP: $\phi_{AMP-ADP} = \dfrac{V_{ADP,AMP}C_{c,ADP}}{(K_{ADP,AMP}+C_{c,ADP})}\dfrac{C_{ADP,c}/C_{ATP,c}}{\mu^{+}_{c}+C_{AMP,c}/C_{ATP,c}}$

[5]AMP to ADO: $\phi_{AMP-ADO} = \dfrac{V_{AMP,ADO}C_{AMP}}{(K_{AMP,ADO}+C_{AMP})}$

[6]ADO to AMP: $\phi_{ADO-AAMP} = \dfrac{V_{ADO,AMP}C_{ADO}}{(K_{ADO,AMP}+C_{ADO})}$

μ or ν (+): C_{ATP}/C_{ADP} or C_{NADH}/C_{NAD} is controller; μ or ν (–): C_{ADP}/C_{ATP} or C_{NAD}/C_{NADH} is controller. $V_{x-y,v-w}$: maximal reaction rate (μmol g^{-1} min^{-1}); $K_{x-y,v-w}$: reaction coefficient (μmol (g ww)$^{-1}$). †$K_{GLY,G6P}$; §$K_{P_i,G6P}$; *coefficient of C_{FADH_2}/C_{FAD} controller. ‡This number is assumed to be proportional to ischaemia level, and here lists the value for 60% ischaemia.

Results

Mitochondrial metabolism

Alterations involved in the electron transport chain and substrate oxidation during ischaemia were evaluated by performing a series of computer simulations (Fig. 2). When myocardial blood flow was reduced from an initial value of 1.0 ml g^{-1} min^{-1} to 0.7, 0.4 and 0.1 ml g^{-1} min^{-1} ('mild', 'moderate' and 'severe' ischaemia), myocardial oxygen consumption decreased 19%, 48% and 86%, respectively (Fig. 2*A*). These values are comparable to experimental data from pigs subjected to flow reductions of 60% (Hacker *et al.* 1994; Stanley *et al.* 1994) and 90% (Ito, 1995). Similar responses to flow reduction were observed for ATP formation from oxidative phosphorylation and for the oxidation of pyruvate and fatty acids (Fig. 2*B–D*), and the TCA cycle (data not shown).

Table 3. Transport flux parameter values under normal, resting steady state

Species	Parameters	
GLU	$M_{b\rightarrow c,GLU} = 4^*$	$T_{b\rightarrow c,GLU} = 0.46$
LAC	$M_{b\rightarrow c,LAC} = 0.10^*$	$T_{b\rightarrow c,LAC} = 0.79$
	$M_{c\rightarrow b,LAC} = 150$	$T_{c\rightarrow b,LAC} = 11.7$
PYR	$M_{c\rightarrow m,PYR} = 0.2$	$T_{c\rightarrow m,PYR} = 1.46$
FFA	$\sigma_{b\leftrightarrow c,FFA} = 7.74$	$\lambda_{b\leftrightarrow c,FFA} = 0.64$
FAC	$M_{c\rightarrow m,FAC} = 0.0084$	$T_{c\rightarrow m,FAC} = 0.28$
O_2	$\sigma_{b\leftrightarrow c,O_2} = 1.0$	$\lambda_{b\leftrightarrow c,O_2} = 5.95$
CO_2	$\sigma_{b\leftrightarrow c,CO_2} = 1.0$	$\lambda_{b\leftrightarrow c,CO_2} = 4.63$
P_i†	$M_{c\leftrightarrow m,P_i} = 3.22$	$T_{c\rightarrow m,P_i} = 94.44$
ATP	$M_{m\rightarrow c,ATP} = 3.22$	$T_{m\rightarrow c,ATP} = 94.44$
ADP	$M_{c\rightarrow m,ADP} = 3.22$	$T_{m\rightarrow c,ADP} = 94.44$
H Leakage	$M^{leakage}_{i\rightarrow m,H} = 250$	$T^{leakage}_{i\rightarrow m,H} = 806.99$
M-A Shuttle	$M_{m\rightarrow c,NAD} = 16.78$	$T_{m\rightarrow c,NAD} = 3.65$
	$M_{c\rightarrow m,NADH} = 0.002$	

M: affinity coefficient (μmol (g ww)$^{-1}$ or mM denoted by*). *T*: normalized transport rate coefficient (μmol min^{-1} (g ww)$^{-1}$). λ: membrane permeability coefficient (min^{-1}). σ: partition coefficient. †Transport rate of P_i is assumed be same as that of ATP.

Table 4. Newly added or modified model parameters or variables

Parameter/variable	Value	Variable	Value
F	0.8	$C_{m,H}$	2.5×10^{-5} mM (Cortassa et al. 2003)
V'_i	0.017	C_{a,O_2}	6.2 mM (current study)
V'_m	0.15	C_{a,O_2}	15.5 mM (Salem et al. 2004)
$C^*_{i,H}$	6.28×10^{-5} mM	$(NADH/NAD^+)_c$	0.05 (Sharma et al. 2005)
$(NADH/NAD^+)_m$	0.24†	C_{AMP}	0.75 nmol (g ww)$^{-1}$
$C_{Adenosine}$	0.5 nmol (g ww)$^{-1}$		

*The intermembrane pH was calculated assuming ΔpH = 0.4 pH unit. †Mitochondrial NADH/NAD$^+$ ratio is calculated from the cytosolic NADH/NAD$^+$ ratio by assuming 90% of total NADH and NAD$^+$ exists in the mitochondria. Parameters or variables were estimated unless noted.

High-energy phosphates metabolism, glycolysis and lactate production

Ischaemia resulted in a decrease in the concentrations of ATP and phosphocreatine. While mild ischaemia did not alter the cytosolic ATP significantly, moderate and severe ischaemia decreased ATP concentration by 53% and 88%, respectively (Fig. 3*A*). Similar dynamic behaviour was observed for the concentration of phosphocreatine (Fig. 3*B*). Concomitantly, the concentrations of cytosolic free ADP (Fig. 3*C*) and P_i (Fig. 3*D*), as well as the cytosolic bound ADP and mitochondrial ADP/ATP (data not shown) increased from their preischaemic values. The increase in cytosolic ADP/ATP with ischaemia triggered net glycogen breakdown (Fig. 4*A*) and activated glycolysis. The rate of glycolysis, which depends on the severity of flow reduction (Fig. 4*B*), was biphasic. It increased sharply with the onset of ischaemia (peaking at 3 min) and then declined to a steady state after 40 min. The accelerated glycolysis during ischaemia resulted in lactate accumulation and production (net lactate release) (Fig. 4*C* and *D*).

Cytosolic and mitochondrial NADH/NAD$^+$

During ischaemia, mitochondrial NADH/NAD$^+$ increased almost as rapidly as $M\dot{V}_{O_2}$ decreased and closely mirrored its response (Fig. 5*A*). Mild, moderate and severe ischaemia caused mitochondrial NADH/NAD$^+$ to increase from its initial value of 0.24 to higher steady-state values of 0.34, 0.62 and 2.62, respectively. During mild ischaemia, cytosolic NADH/NAD$^+$ followed a pattern similar to that of mitochondrial NADH/NAD$^+$ although with a slight biphasic behaviour (Fig. 5*B*). With moderate and severe ischaemia, however, cytosolic NADH/NAD$^+$ increased severalfold from an initial value of 0.05 to peak values of 0.29 and 0.69, respectively, 3 min after onset

of ischaemia. Then, this ratio decreased to steady-state values of 0.13 and 0.18, respectively. The rate of NADH transport *via* the malate–aspartate shuttle also decreased rapidly with the onset of ischaemia. The transport rate was reduced by 26%, 56% and 89% with flow reductions of 30, 60 and 90% (Fig. 5*C*).

Effects of initial glycogen concentration and malate–asparate shuttle activity

Two *in silico* experiments were implemented under moderate ischaemic condition (60% reduction in blood flow) to further study the mechanism involved in the differential regulation of NADH/NAD$^+$ in cytosol and mitochondria and test our hypotheses. Changing glycogen initial concentration (preischaemic glycogen concentration) affected the dynamics of cytosolic NADH/NAD$^+$ and lactate production during the initial period of ischaemia (Fig. 6), but it had no effect on mitochondrial NADH/NAD$^+$, nor on the steady state values for cytosolic NADH/NAD$^+$ or lactate production at 60 min (Fig. 6). Doubling the initial glycogen concentration increased the peak cytosolic NADH/NAD$^+$ (from 0.28 to 0.3) and lactate production (from 0.7 to 0.8), which were followed by a slower decrease to new steady states. When the glycogen initial concentration was decreased by half, the cytosolic NADH/NAD$^+$ and lactate production decreased faster (Fig. 6*A* and *C*). The mitochondrial NADH/NAD$^+$ were identical with different glycogen initial concentrations (Fig. 6*B*), as well as the rate of the malate–aspartate shuttle (data not shown). Thus the rate of glycogen breakdown is a major determinant of cytosolic NADH/NAD$^+$ and lactate production with the onset of ischaemia, but clearly does not effect mitochondrial metabolism or steady state values of lactate production.

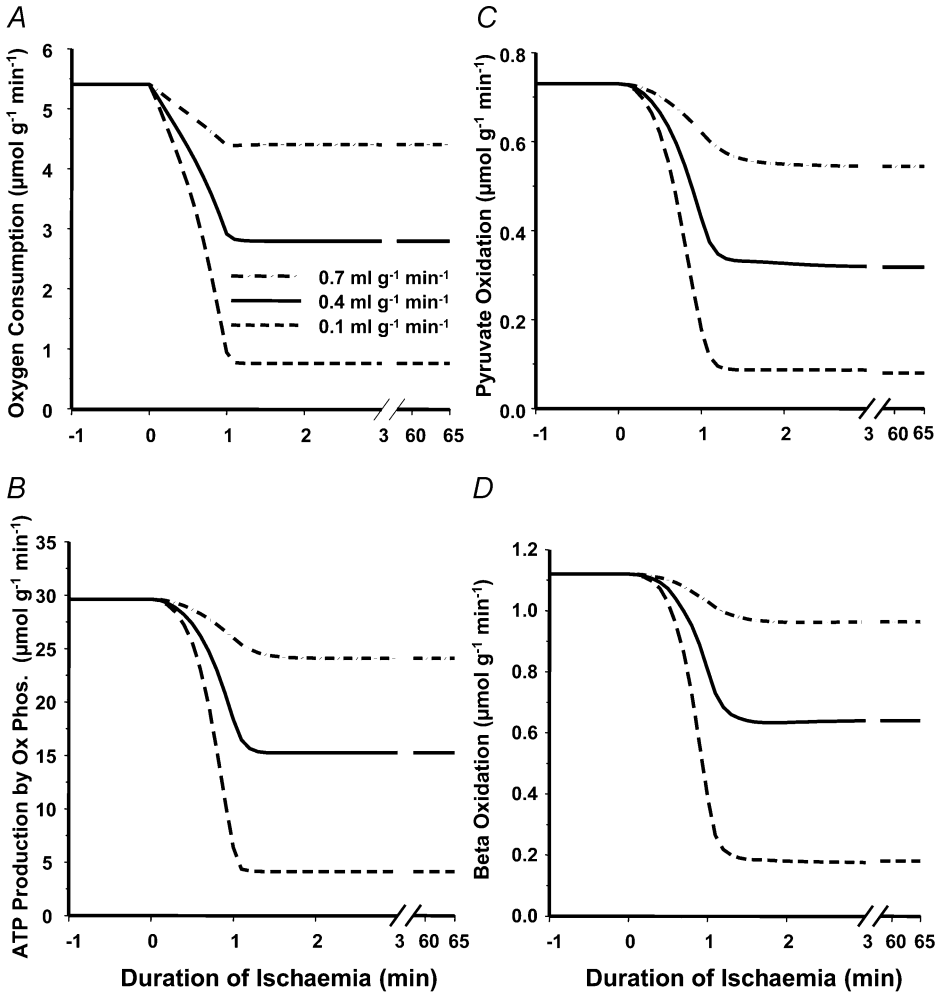

Figure 2
Model simulated dynamics of myocardial oxygen consumption (*A*), ATP generation by oxidative phosphorylation (*B*), pyruvate oxidation (*C*), and fatty acids oxidation (*D*) in response to mild (0.7 ml g^{-1} min^{-1}), moderate (0.4 ml g^{-1} min^{-1}) and severe ischaemia (0.1 ml g^{-1} min^{-1}).

A fourfold increase or an 80% decrease in the malate–aspartate shuttle activity affected cytosolic NADH/NAD^+ and lactate production noticeably, but affected mitochondrial NADH/NAD^+ only a little (Fig. 7). A decrease of shuttle activity by 80% increased cytosolic NADH/NAD^+ significantly both in the peak value (from 0.28 to 0.29) and steady state (from 0.13 to 0.15). Also, increased shuttle activity decreased cytosolic NADH/NAD^+ significantly. Similar results were found under mild and severe ischaemic conditions (data not shown). Thus, the capacity to transfer NADH from the cytosol to the mitochondrial is a key controller of lactate production both in the initial phase of ischaemia and during the steady state.

Discussion

The novel finding of this study is that lactate production during the initial period of ischaemia is not determined directly by the mitochondrial NADH/NAD^+, but rather by the cytosolic NADH/NAD^+. In addition, the transfer of NADH into the mitochondria via the malate–aspartate shuttle is a key regulator of the cytosolic NADH/NAD^+ and lactate production, but has only minor effects on mitochondrial NADH/NAD^+. These results, which cannot be obtained using existing experimental methods, demonstrate the utility of computational models in the investigation of the role of metabolic compartmentation in the regulation of cellular energy metabolism.

Model validation

With a 60% reduction in myocardial blood flow, the model simulations corresponded closely with available experimental data on oxygen consumption (Fig. 2*A*, experimental data not shown) (Hall *et al.* 1996), glycogen (Fig. 4*A*) and lactate (Fig. 4*C*) concentrations, as well as lactate production (Fig. 4*D*) (Salem *et al.* 2004). Ischaemia causes a decrease in oxidative phosphorylation and ATP generation, which inhibits pyruvate and fatty acids oxidation (Fig. 2) and increases the reliance on anaerobic glycolysis (Taegtmeyer, 1994). Experimental studies have

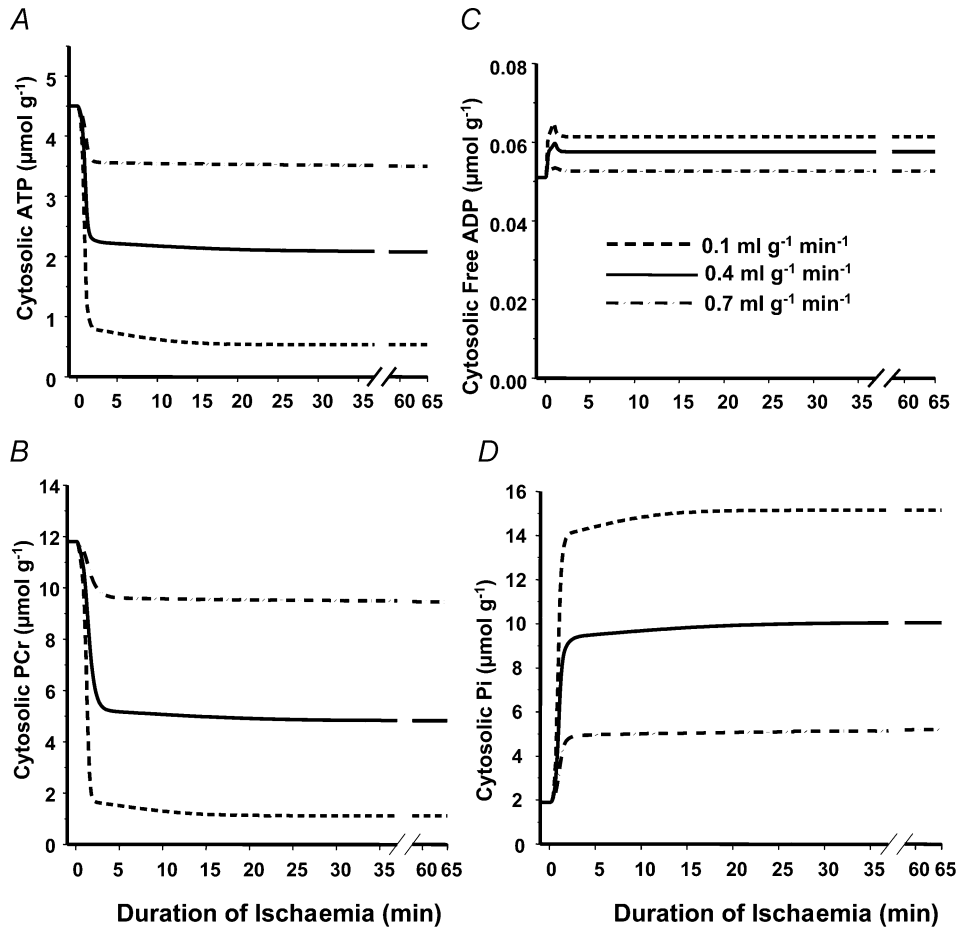

Figure 3
Model simulated dynamics of cytosolic ATP (*A*), PCr (*B*), free ADP (*C*), and P_i (*D*) in response to mild (0.7 ml g^{-1} min^{-1}), moderate (0.4 ml g^{-1} min^{-1}) and severe ischaemia (0.1 ml g^{-1} min^{-1}).

shown that with the onset of moderate ischaemia there is an exponential decrease in glycogen concentration, rapid accumulation of lactate, and a switch from net lactate uptake to lactate production (Arai *et al.* 1991; Stanley *et al.* 1996), as predicted by our model. Consistent with a depletion of high-energy phosphates observed in pig experiments with moderate ischaemia (Pantley *et al.* 1990; Arai *et al.* 1991), our simulations show a decrease in the concentrations of cytosolic ATP and PCr, and an increase on the concentration of cytosolic P_i.

Effect of ischaemia on cytosolic and mitochondrial NADH/NAD$^+$

The dynamic responses of cytosolic and mitochondrial NADH/NAD$^+$ differed during the transition from normal to ischaemic conditions, especially with severe ischaemia (Fig. 5). While mitochondrial NADH/NAD$^+$ increased rapidly in a step-like manner with the onset of ischaemia, cytosolic NADH/NAD$^+$ had a biphasic behaviour in response to ischaemia. The ischaemic steady-state values of NADH/NAD in the mitochondria and cytosol were also significantly different relative to their initial values under normal conditions. This suggests that cytosolic and mitochondrial NADH/NAD$^+$ are determined by different processes activated by ischaemia. Mitochondrial NADH/NAD$^+$ changes closely parallel those of $M\dot{V}_{O_2}$ and blood flow (Figs 2*A* and 5*A*). A reasonable interpretation is that a decrease in $M\dot{V}_{O_2}$ inhibits the rate of mitochondrial NADH oxidation through complex I in the electron transport chain. In turn, this lowers the rate of NADH utilization relative to NADH production by mitochondrial dehydrogenases and leads to NADH accumulation. Such a sequence of events supports the hypothesis that changes in mitochondrial NADH/NAD$^+$ are secondary to changes in myocardial oxygen consumption (Ashruf *et al.* 1995). In addition, changes in glycogen storage and glycolytic rate had no effect on mitochondrial NADH/NAD$^+$

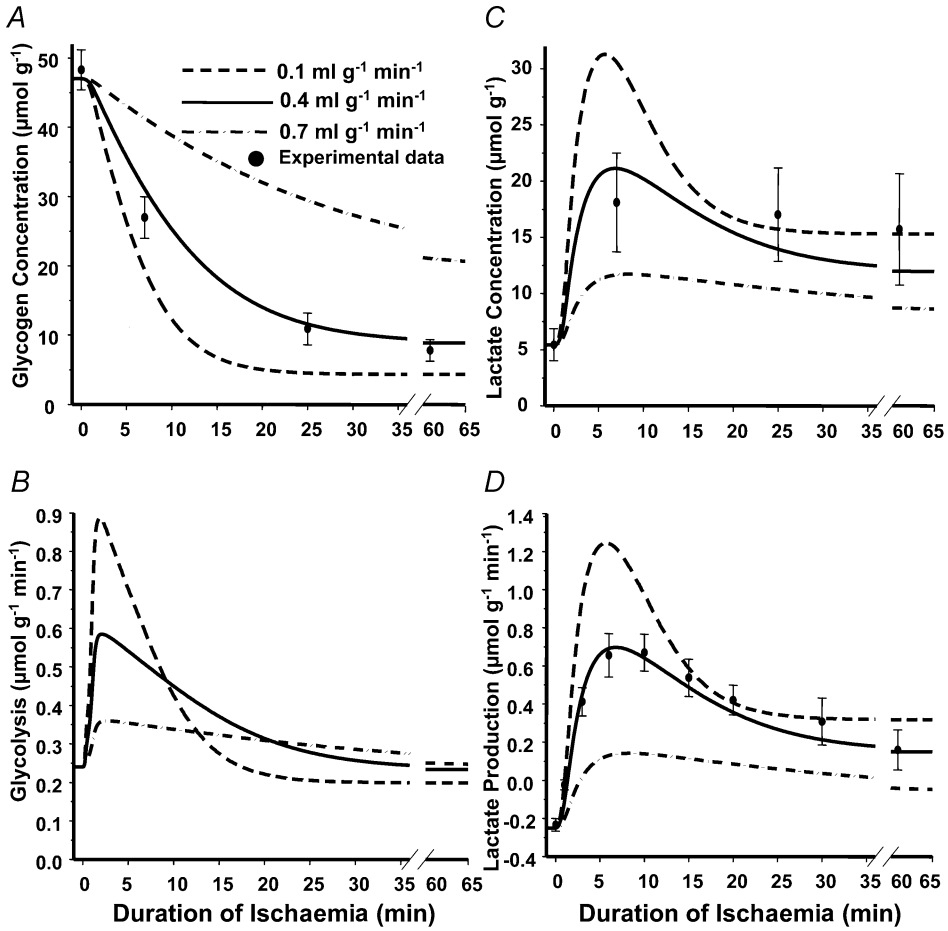

Figure 4
Model simulated dynamics of glycogen concentration (*A*), glycolysis (*B*), lactate concentration (*C*), and lactate production (*D*) in response to mild (0.7 ml g^{-1} min^{-1}), moderate (0.4 ml g^{-1} min^{-1}) and severe ischaemia (0.1 ml g^{-1} min^{-1}). Filled circles represent experimental data on glycogen concentration, lactate concentration and lactate production (Salem *et al.* 2004).

(Fig. 6*B*) suggesting that the regulation of mitochondrial NADH/NAD$^+$ is localized in this compartment during ischaemia.

Cytosolic NADH/NAD$^+$, however, is determined primarily by the rates of glycogen breakdown and glycolysis, and secondarily by the rate of oxygen consumption through the malate–aspartate shuttle during blood flow reduction. Ischaemia activates glycogen breakdown and accelerates glycolysis (Fig. 4*A* and *B*) to produce more NADH through glyceraldhyde-3-phosphate dehydrogenase. However, during ischaemia the rate of NADH being transferred into the mitochondria decreases (Fig. 5*C*) due to the inhibition of the electron transport chain by lower oxygen availability. Consequently, NADH derived from glycolysis cannot be transported into mitochondria at the same rate as under normal conditions, which leads to NADH accumulation inside the cytosol. As glycogen is depleted, the glycolytic rate decreases toward its initial value (Fig. 4*B*), resulting in the biphasic behaviour of cytosolic NADH/NAD$^+$ (Fig. 5*B*). This relationship between glycolysis and cytosolic NADH/NAD$^+$ is also supported by the high correlation between them (data not shown), as well as by *in silico* experimental results obtained with different glycogen initial concentrations (Fig. 6*A*).

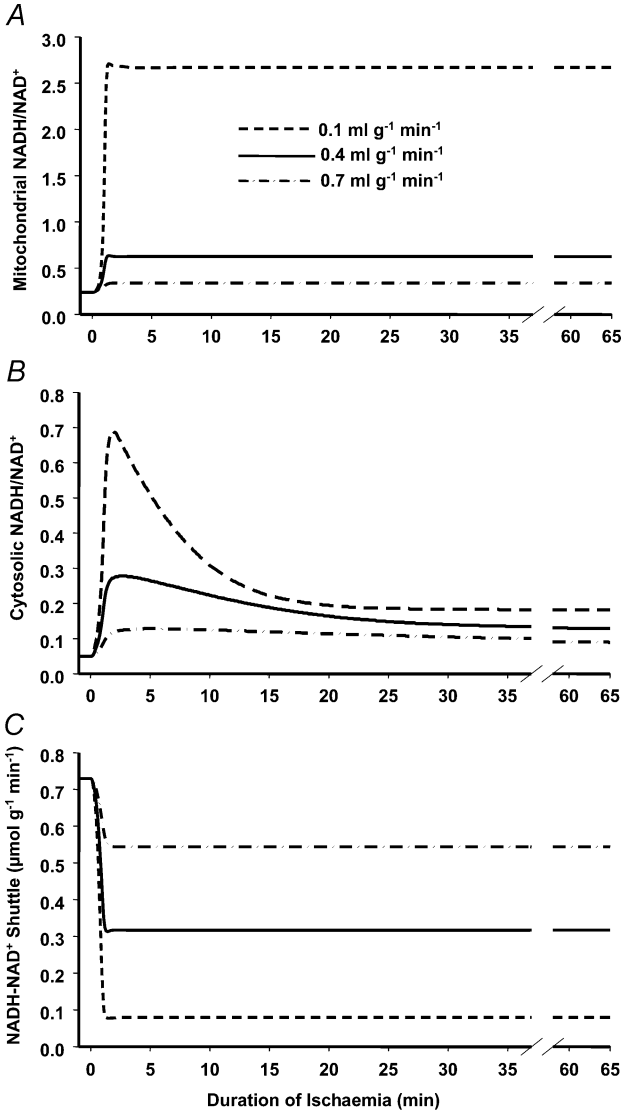

Figure 5
Computer simulated values of mitochondrial NADH to NAD$^+$ ratio (*A*), cytosolic NADH to NAD$^+$ ratio (*B*), and rate of malate–aspartate shuttle (*C*) during mild (0.7 ml g^{-1} min^{-1}), moderate (0.4 ml g^{-1} min^{-1}) and severe ischaemia (0.1 ml g^{-1} min^{-1}).

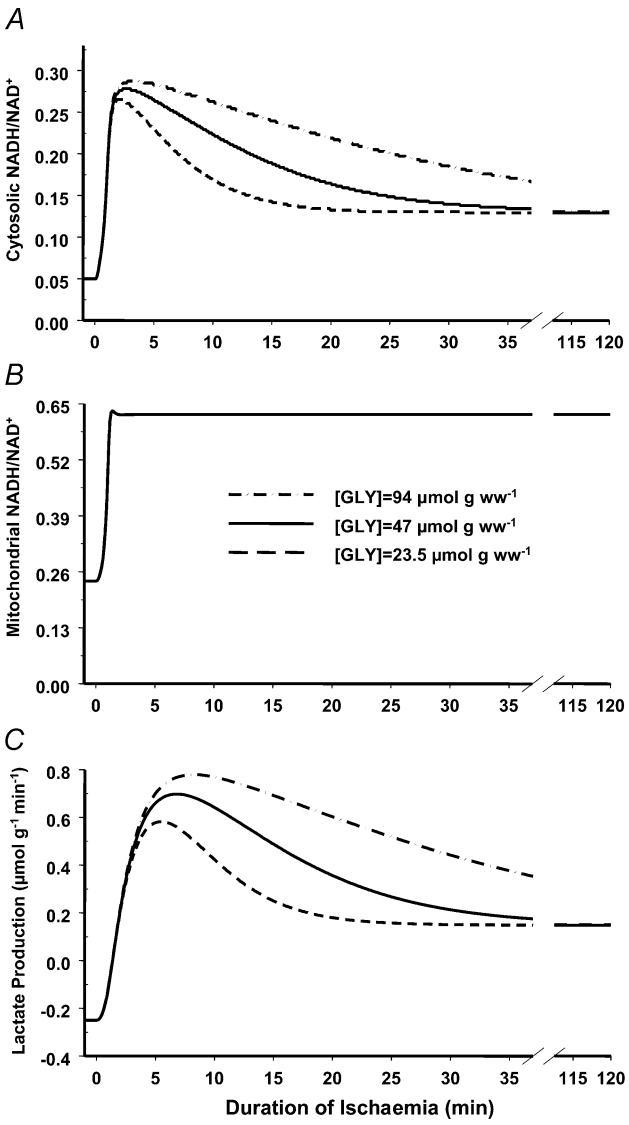

Figure 6
Effects of glycogen storage on the dynamics of cytosolic NADH/NAD$^+$ (*A*), mitochondrial NADH/NAD$^+$ (*B*), and lactate production (*C*) in response to moderate (0.4 ml g^{-1} min^{-1}) ischaemia.

Compartmentation of cytosolic and mitochondrial metabolism

Corresponding to the differential behaviours of cytosolic and mitochondrial NADH/NAD$^+$ dynamics during blood flow reduction, our results demonstrate that during ischaemia the role of NADH/NAD$^+$ is localized, and modulates primarily the processes that occur in the same subcellular compartment. The overall behaviour of net lactate production in response to ischaemia is similar to that of cytosolic NADH/NAD$^+$ (Figs 4 and 5). This implies that the rate of lactate production is largely controlled by the rates of glycolysis and glycogenolysis, and modulated by the cytosolic NADH/NAD$^+$. In the mitochondria, NADH/NAD$^+$ displays ischaemic responses similar to those of pyruvate and fatty acid oxidation and the TCA cycle, which implies that it modulates these processes. Previous studies (Hansford & Cohen, 1978; Stanley *et al.* 1997) indicate that the primary regulator of pyruvate oxidation through pyruvate dehydrogenase (PDH) is the mitochondrial NADH/NAD$^+$. Similarly, mitochondrial β-oxidation appears to depend primarily on mitochondrial NADH/NAD$^+$, which determines the rate of 1-hydroxyacyl-CoA dehydrogenase (Jafri *et al.* 2001). *In silico* studies here show that reduced oxidative phosphorylation increases mitochondrial NADH/NAD$^+$ immediately, and pyruvate oxidation and β-oxidation decrease within 1 min in a step-like manner. None of the cytosolic metabolic processes coupled to NADH/NAD$^+$ displayed a dynamic response that resembled that of mitochondrial NADH/NAD$^+$.

Cellular metabolic communication during ischaemia

Although the metabolic processes in the cytosol and mitochondria are controlled locally, communication between them is necessary to achieve optimal substrate utilization, as well as to maintain a balance between ATP production and utilization. Under normal conditions, net NADH production occurs in the cytosol through glycolysis and lactate oxidation. This leads to the transport of NADH into the mitochondria where it is oxidized by complex I. At the same time, the mitochondrial-generated NAD$^+$ must be transported into the cytosol since it is needed for glycolysis. Because the inner mitochondrial membrane is not permeable to nicotinamide adenine dinucleotides, the transport of NADH and NAD$^+$ cannot take place by simple diffusion. In myocardium, NADH transport into the mitochondria in exchange for NAD$^+$ is accomplished by the malate–aspartate shuttle. This shuttle is a complex system including two complementary cytosolic and mitochondrial redox and transamination reactions and two transporters that span the inner mitochondrial membrane, i.e. the malate–α-ketoglutarate transporter and glutamate–aspartate transporter (Arnold, 1992). The electrogenic glutamate–aspartate transporter is considered to represent the rate-limiting step of the malate–aspartate shuttle (LaNoue & Tischler, 1974).

The malate–aspartate shuttle may provide an important mechanism to regulate metabolic activity in subcellular compartments. Studies on isolated mitochondria show that hyperthyroid-induced left ventricular (LV) hypertrophy can lead to an increase in shuttle capacity (Scholz *et al.* 2000). Also, dynamic ^{13}C NMR spectroscopy has revealed depressed metabolite transport in postischaemic hearts (Lewandowski *et al.* 1997). However, it is difficult to elucidate the impact of altered malate–aspartate shuttle activity on cellular metabolism from experimental studies.

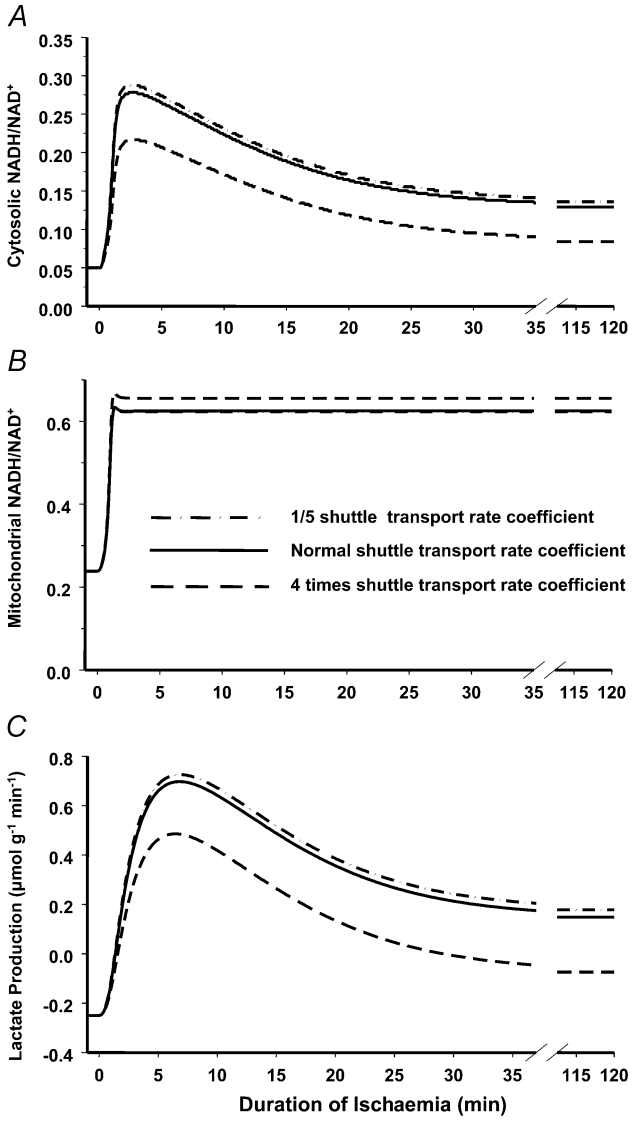

Figure 7
Effects of malate–aspartate shuttle activity on the dynamics of cytosolic NADH/NAD$^+$ (*A*), mitochondrial NADH/NAD$^+$ (*B*), and lactate production (*C*) in response to moderate (0.4 ml g^{-1} min^{-1}) ischaemia.

The isolated mitochondria approach focuses on the efflux of metabolites from the mitochondria to an artificial cytosolic environment. It therefore cannot elucidate the interaction between two metabolic compartments. Although ^{13}C spectroscopy allows the characterization of metabolic activity and metabolite transport in intact tissue, the low temporal resolution renders it inadequate to study transient responses during sudden changes in pathophysiological conditions.

This *in silico* study is the first to show that the cytosolic NADH transport into the mitochondria is a key controller of the cytosolic NADH/NAD^+ and lactate production at a given level of myocardial ischaemia. Simulations show that a 30% reduction in blood flow decreases the shuttle rate by 26%, while a 90% reduction decreases the shuttle rate by 89% (Fig. 5*C*). This indicates that ischaemia impairs the ability of the malate–aspartate shuttle to translocate NADH and NAD^+ between cytosol and mitochondria, which is consistent with experimental observations (Lewandowski *et al.* 1997). Since the rates of the ATP–ADP translocation, and pyruvate and fatty acyl-CoA transport into the mitochondria decreased similarly in response to blood flow reduction (data not shown), as well as the correlation between cytosolic NADH/NAD^+ and mitochondrial metabolism being lower during ischaemia, we surmise that cytosol–mitochondria metabolic communication is impaired during ischaemia.

Model limitations and future directions

In this study, we modified our previously published model of cardiac metabolism (Cabrera *et al.* 2005; Zhou *et al.* 2005) during ischaemia by incorporating the mitochondrial electron transport chain and oxidative phosphorylation. Although there are no significant differences in the simulation results for oxygen consumption, glycogen breakdown and lactate production between these two models, separating these two processes and including $FADH_2$ have made the model more mechanistic in order to mimic more closely the cellular processes observed experimentally. Moreover, this enhancement will be critical for modelling cardiac metabolism with other physiological and pathological stresses (e.g. exercise, hypoxia) in the future, where the respiratory chain and oxidative phosphorylation may be controlled and activated by different mechanisms (Balaban *et al.* 2003).

While the current model is more comprehensive than previous ones, it still has several limitations that need to be addressed. (1) Since our model has only a minimal representation of the malate–aspartate shuttle (Fig. 1) based on limited experimental data, many details of the processes comprising the shuttle system cannot be examined. To elucidate more accurately the effects of metabolic communication on the differential regulation of cytosolic and mitochondrial energy metabolism, a refined model that incorporates more key components of the shuttle is needed together with appropriate experimental data for validation. (2) Another simplification in our model is the lack of transport of lactate into mitochondria and the localization of lactate dehydrogenase (LDH) solely to the cytosol, despite evidence for LDH activity in mitochondria (Brooks *et al.* 1999). The evidence for mitochondrial LDH comes from histological assessments and from studies on isolated mitochondria (Brooks, 2002). Thus it is difficult to assign an activity to mitochondrial LDH in our model. It is possible, however, that a significant portion of the pyruvate generation occurs in the mitochondria via the oxidation of lactate. (3) Our current model treats the intracellular space as a well-mixed chamber, assuming uniform oxygen concentration in all mitochondria. However, even during ischaemia, there is an O_2 concentration gradient from the capillary to the centre of the myocyte, which suggests that the oxygen concentration is higher in subsarcolemmal mitochondria than in the intrafibrillar population (Lesnefsky *et al.* 2001). Future studies should consider these differences. (4) Our model does not include cellular acidification during ischaemia, which can adversely affect contractile function and glycolytic flux (Stanley *et al.* 2005; Stanley *et al.* 1997). Our future model should incorporate cytosolic H^+ metabolism.

Summary

Our *in silico* studies of acute myocardial ischaemia imply that during ischaemia cytosolic and mitochondrial NADH/NAD^+ have significantly different behaviours controlled by different metabolic processes. While mitochondrial NADH/NAD^+ is determined mainly by the myocardial oxygen delivery, cytosolic NADH/NAD^+ is primarily determined by glycogen breakdown and glycolysis, and secondarily by oxygen consumption via the malate–aspartate shuttle. In addition, these NADH/NAD^+ ratios also play different roles in the regulation of cardiac energy metabolism. Mitochondrial NADH/NAD^+ affects the rates of pyruvate and fatty acids oxidation while the cytosolic NADH/NAD^+ modulates the rate of lactate metabolism.

References

Arai AE, Pantley GA, Anselone CG, Bristow J & Bristow JD (1991). Active downregulation of myocardial energy requirements during prolonged moderate ischemia in swine. *Circ Res* **69**, 1458–1469.

Arnold M (1992). *Physiology of the Heart*, 2nd edn, Raven Press, New York.

Ashruf JF, Coremans JM, Bruining HA & Ince C (1995). Increase of cardiac work is associated with decrease of mitochondrial NADH. *Am J Physiol* **269**, H856–H862.

Balaban RS, Bose S, French SA & Territo PR (2003). Role of calcium in metabolic signaling between cardiac sarcoplasmic reticulum and mitochondria in vitro. *Am J Physiol Cell Physiol* **284**, C285–C293.

Brooks GA (2002). Lactate shuttles in nature. *Biochem Soc Trans* **30**, 258–264.

Brooks GA, Dubouchaud H, Brown M, Sicurello JP & Butz CE (1999). Role of mitochondrial lactate dehydrogenase and lactate oxidation in the intracellular lactate shuttle. *Proc Natl Acad Sci U S A* **96**, 1129–1134.

Cabrera ME, Zhou L, Stanley WC & Saidel GM (2005). Regulation of cardiac energetics: role of redox state and cellular compartmentation during ischemia. *Ann N Y Acad Sci* **1047**, 259–270.

Cortassa S, Aon MA, Marban E, Winslow RL & O'Rourke B (2003). An integrated model of cardiac mitochondrial energy metabolism and calcium dynamics. *Biophys J* **84**, 2734–2755.

Hacker TA, Renstrom B, Paulson D, Liedtke AJ & Stanley WC (1994). Ischemia produces an increase in ammonia output in swine myocardium. *Cardioscience* **5**, 255–260.

Hall J, Lopaschuk G, Barr A, Bringas J, Pizzurro R & Stanley WC (1996). Increased cardiac fatty acid uptake with dobutamine infusion in swine is accompanied by a decrease in malonyl CoA levels. *Circ Res* **32**, 879–885.

Hansford R & Cohen L (1978). Relative importance of pyruvate dehydrogenase interconversion and feed-back inhibition in the effect of fatty acids on pyruvate oxidation by rat heart mitochondria. *Arch Biochem Biophys* **191**, 65–81.

Horton H, Moran L, Ochs S, Rawn J & Scrimgeour K (2002). *Principles of Biochemistry*. Prentice Hall, Upper Saddle River, NJ.

Ingwall JS (2002). *ATP and the Heart*. Kluwer Academic Publishers, Boston/Dordrecht/London.

Ito B (1995). Gradual onset of myocardial ischemia results in reduced myocardial infarction: association with reduced contractile function and metabolic downregulation. *Circulation* **91**, 2058–2070.

Jafri MS, Dudycha SJ & O'Rourke B (2001). Cardiac energy metabolism: models of cellular respiration. *Annu Rev Biomed Eng* **3**, 57–81.

Korzeniewski B (2000). Regulation of ATP supply in mammalian skeletal muscle during resting state → intensive work transition. *Biophys Chem* **83**, 19–34.

Korzeniewski B, Noma A & Matsuoka S (2005). Regulation of oxidative phosphorylation in intact mammalian heart in vivo. *Biophys Chem* **116**, 145–157.

LaNoue KF & Tischler ME (1974). Electrogenic characteristics of the mitochondrial glutamate-aspartate antiporter. *J Biol Chem* **249**, 7522–7528.

Lesnefsky EJ, Gudz TI, Moghaddas S, Migita CT, Ikeda-Saito M, Turkaly PJ & Hoppel CL (2001). Aging decreases electron transport complex III activity in heart interfibrillar mitochondria by alteration of the cytochrome c binding site. *J Mol Cell Cardiol* **33**, 37–47.

Lewandowski ED, Yu X, LaNoue KF, White LT, Doumen C & O'Donnell JM (1997). Altered metabolite exchange between subcellular compartments in intact postischemic rabbit hearts. *Circ Res* **81**, 165–175.

Pantley G, Malone S, Rhen W, Anselone C, Arai A & Bristow J (1990). Regeneration of myocardial phosphocreatine in pigs despite continuted moderate ischemia. *Circ Res* **67**, 1491–1493.

Salem J, Cabrera M, Chandler M, McElfresh T, Huang H, Sterk J & Stanley WC (2004). Step and ramp induction of myocardial ischemia: comparison of in vivo and in silico results. *J Physiol Pharmcol* **55**, 519–536.

Scholz TD, TenEyck CJ & Schutte BC (2000). Thyroid hormone regulation of the NADH shuttles in liver and cardiac mitochondria. *J Mol Cell Cardiol* **32**, 1–10.

Sharma N, Okere IC, Brunengraber DZ, McElfresh TA, King KL, Sterk JP, Huang H, Chandler MP & Stanley WC (2005). Regulation of pyruvate dehydrogenase activity and citric acid cycle intermediates during high cardiac power generation. *J Physiol* **562**, 593–603.

Stanley WC, Hall JL, Smith KR, Cartee GD, Hacker TA & Wisneski JA (1994). Myocardial glucose transporters and glycolytic metabolism during ischemia in hyperglycemic diabetic swine. *Metabolism* **43**, 61–69.

Stanley W, Hall J, Stone C & Hacker T (1992). Acute myocardial ischemia causes a transmural gradient in glucose extraction but not glucose uptake. *Am J Physiol* **262**, H91–H96.

Stanley W, Hernandez L, Spires D, Bringas J, Wallace S & McCormack J (1996). Pyruvate dehydrogenase activity and malonyl CoA levels in normal and ischemic swine myocardium: effects of dichloroacetate. *J Mol Cell Cardiol* **28**, 905–914.

Stanley W, Lopaschuk G, Hall J & McCormack J (1997). Regulation of myocardial carbohydrate metabolism under normal and ischemic conditions. *Cardiovascular Res* **33**, 243–257.

Stanley WC, Recchia FA & Lopaschuk GD (2005). Myocardial substrate metabolism in the normal and failing heart. *Physiol Rev* **85**, 1093–1129.

Taegtmeyer H (1994). Energy metabolism of the heart: from basic concepts to clinical applications. *Curr Probl Cardiol* **19**, 59–113.

Williamson JR, Schaffer SW, Ford C & Safer B (1976). Contribution of tissue acidosis to ischemic injury in the perfused rat heart. *Circulation* **53**, I3–I14.

Zhou L, Salem JE, Saidel GM, Stanley WC & Cabrera ME (2005). Mechanistic model of cardiac energy metabolism predicts localization of glycolysis to cytosolic subdomain during ischemia. *Am J Physiol Heart Circ Physiol* **288**, H2400–H2411.

Acknowledgements

This work was support by a grant from the NIH National Institute of General Medical Sciences (P50 G-66309), which established the Center for Modelling Integrated Metabolic Systems (MIMS) at Case Western Reserve University. The complete model can be found at MIMS website http://www.csuohio.edu/mims.